# **Supplementary Information** for Interaction of Natural Flavonoid Eriocitrin with β-Cyclodextrin and Hydroxypropyl-β-Cyclodextrin: an NMR and Molecular Dynamics Investigation

Andrea Cesari[1], Gloria Uccello Barretta[1], Karl N. Kirschner[*2], Matteo Pappalardo[3], Livia Basile[3], Salvatore Guccione[†3], Clizia Russotto[‡3], Maria Rosaria Lauro[4], Francesca Cavaliere[5], and Federica Balzano[§1]

[1]Department of Chemistry and Industrial Chemistry, University of Pisa, Via G. Moruzzi 13, I-56124 Pisa, Italy
[2]Department of Computer Science, University of Applied Sciences Bonn-Rhein-Sieg, Grantham-Allee 20, D-53757 Sankt Augustin, Germany
[3]Department of Drug Sciences, University of Catania, Viale Andrea Doria, 6, I-95125 Catania, Italy
[4]Department of Pharmacy, University of Salerno, Via Giovanni Paolo II, I-84084 Fisciano (SA), Italy
[5]Molecular Modelling Laboratory, Department of Food and Drug, University of Parma, Parco Area delle Scienze 11/A, I-43124 Parma, Italy

September 2, 2020

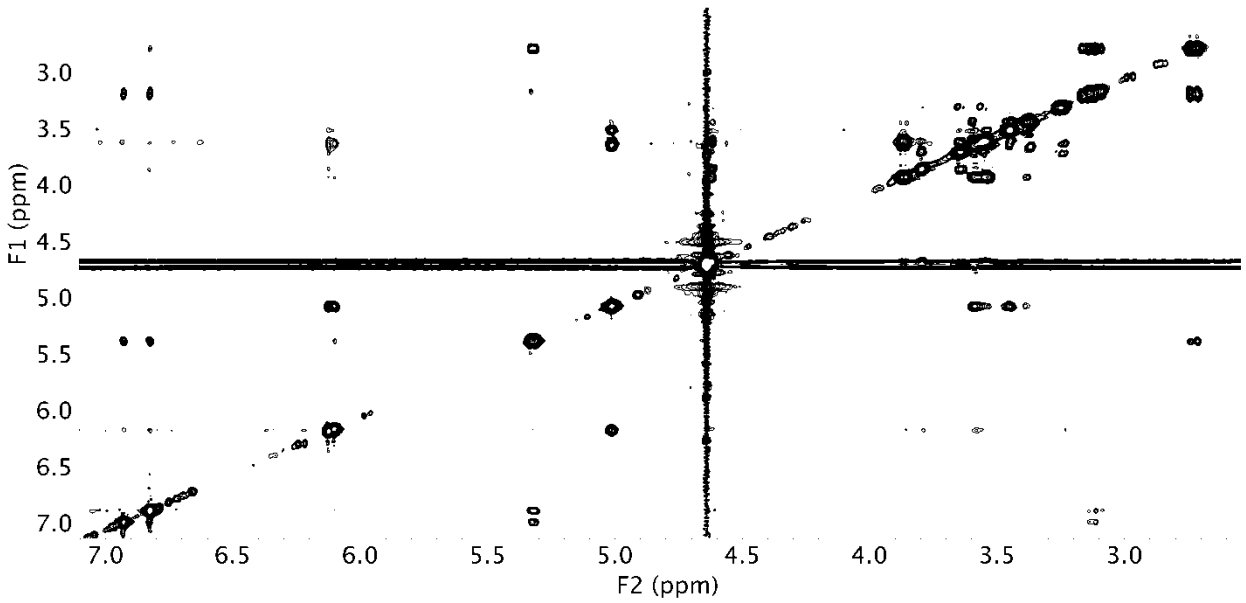


**Figure S1** Portion of 2D ROESY map (600 MHz, $D_2O$, 25 °C) of ERT.

[*]Corresponding author: karl.kirschner@h-brs.de
[†]Corresponding author: guccione@unict.it
[‡]Current affiliation: Department of Chemical Biology-Faculty of Health Sciences-UiT The Arctic University of Norway, Hansine Hansens veg.9019 Tromsø, Norway.
[§]Corresponding author: federica.balzano@unipi.it

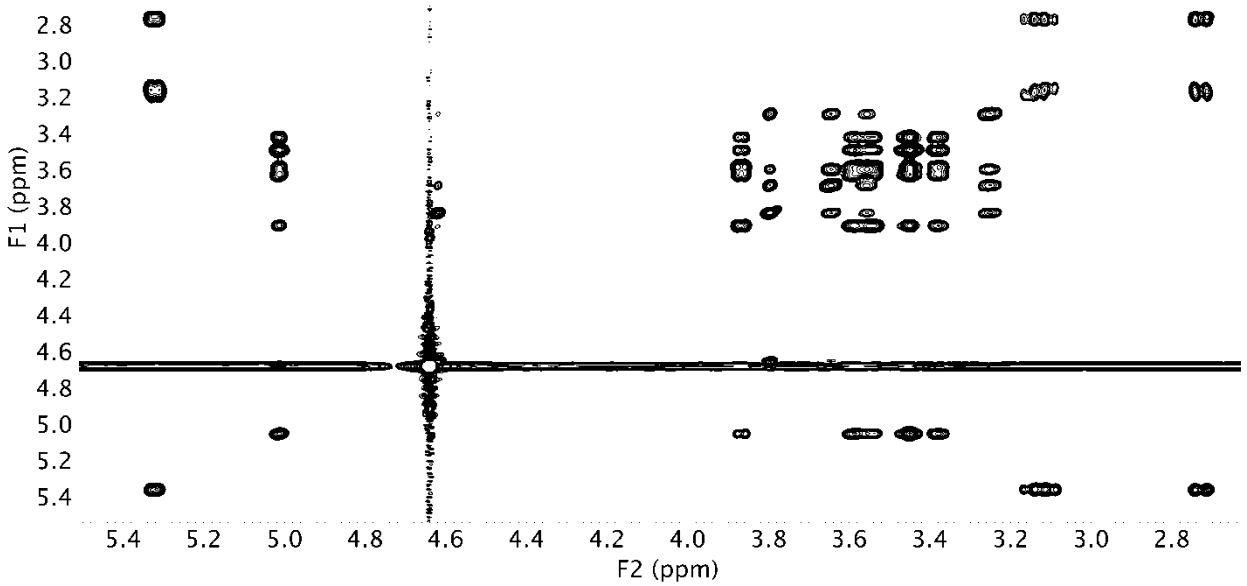


**Figure S2** Portion of 2D TOCSY map (600 MHz, $D_2O$, 25 °C) of ERT.

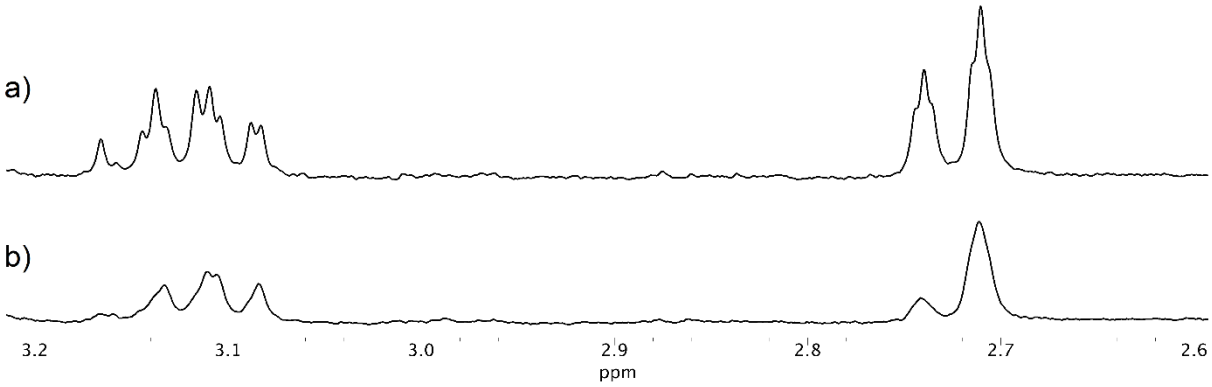


**Figure S3** $^1$H NMR (600 MHz, $D_2O$, 25 °C) spectral region of $H_3^{ERT\text{-}C}$ protons (a) freshly prepared and (b) after 20 days.

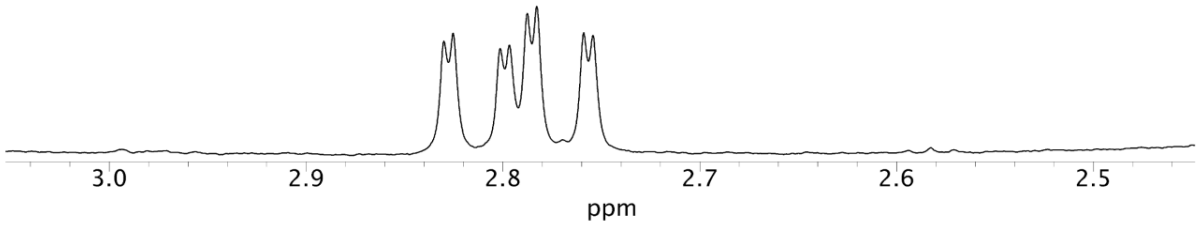


**Figure S4** $^1$H NMR (600 MHz, $CD_3CN$, 25 °C) spectral region including $H_3^{ERT\text{-}C}$.

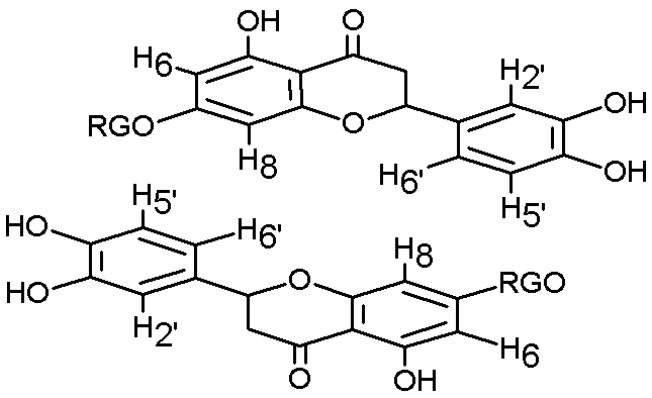


**Figure S5** Supramolecular disposition of two molecules of ERT in an anti-parallel arrangement; G = glucose unit, R = rhamnose unit.

**Table S1** $^{1}$H NMR (600 MHz, $D_2O$, 25 ℃) chemical shifts (ppm) of ERT (1.53 mM).

| A, B and C protons | ppm | G protons | ppm | R protons | ppm |
|---|---|---|---|---|---|
| $H_{2'}^{ERT\text{-}B}$ | 6.93 | $H_{1}^{ERT\text{-}G}$ | 5.019/5.006 | $H_{1}^{ERT\text{-}R}$ | 4.622 |
| $H_{5'}^{ERT\text{-}B}$ | 6.825 | $H_{6}^{ERT\text{-}G}$ | 3.873 | $H_{2}^{ERT\text{-}R}$ | 3.797 |
| $H_{6'}^{ERT\text{-}B}$ | 6.825 | $H_{5}^{ERT\text{-}G}$ | 3.59 | $H_{3}^{ERT\text{-}R}$ | 3.645 |
| $H_{2}^{ERT\text{-}C}$ | 5.32 | $G_{6'}^{ERT\text{-}G}$ | 3.543 | $H_{5}^{ERT\text{-}R}$ | 3.557 |
| $H_{3}^{ERT\text{-}C}$ | 3.12/2.73 | $H_{2}^{ERT\text{-}G} + H_{3}^{ERT\text{-}G}$ | 3.46 | $H_{4}^{ERT\text{-}R}$ | 3.251 |
| $H_{8}^{ERT\text{-}A}$ | 6.12 | $H_{4}^{ERT\text{-}G}$ | 3.378 | $H_{6}^{ERT\text{-}R}$ | 1.035/1.023 |
| $H_{6}^{ERT\text{-}A}$ | 6.1 | | | | |

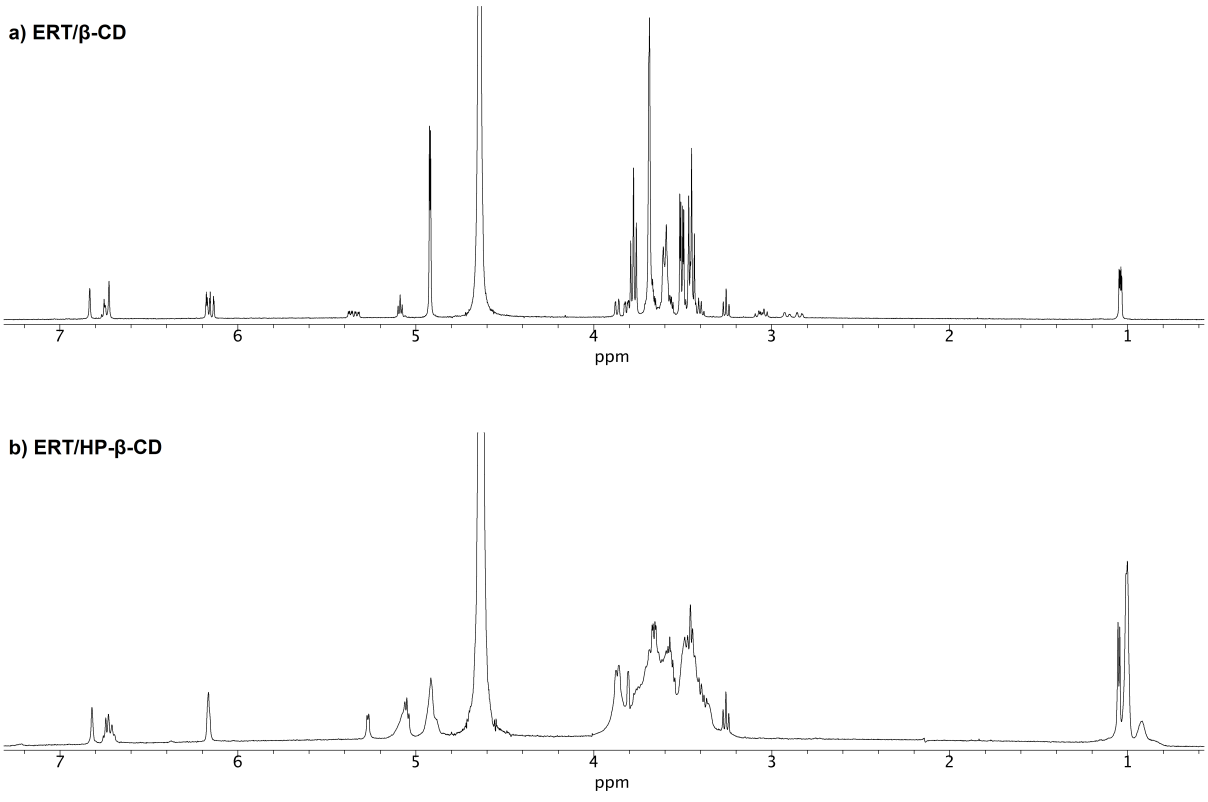


**Figure S6** $^{1}$H NMR (600 MHz, $D_2O$, 25 ℃) spectrum of a) ERT/β-CD 1:1 and b) ERT/HP-β-CD 1:1.

**Table S2** $^1$H NMR (600 MHz, $D_2O$, 25 °C) complexation shifts ($\Delta\delta$, ppm) of ERT (1.53 mM) in ERT/β-CD 1:1 mixture. (* nd = not determined).

| A, B and C protons | $\Delta\delta$ (ppm), I/II | G protons | $\Delta\delta$ (ppm) | R protons | $\Delta\delta$ (ppm) |
|---|---|---|---|---|---|
| $H_{2'}^{ERT\text{-}B}$ | -0.096 | $H_1^{ERT\text{-}G}$ | nd* | $H_1^{ERT\text{-}R}$ | 0.005 |
| $H_{5'}^{ERT\text{-}B}$ | -0.101/-0.069 | $H_6^{ERT\text{-}G}$ | -0.004 | $H_2^{ERT\text{-}R}$ | 0.020 |
| $H_{6'}^{ERT\text{-}B}$ | -0.101/-0.089 | $H_5^{ERT\text{-}G}$ | nd* | $H_3^{ERT\text{-}R}$ | 0.027 |
| $H_2^{ERT\text{-}C}$ | 0.050/0.013 | $G_{6'}^{ERT\text{-}G}$ | 0.036 | $H_5^{ERT\text{-}R}$ | 0.031 |
| $H_3eq^{ERT\text{-}C}$ | nd* | $H_2^{ERT\text{-}G} + H_3^{ERT\text{-}G}$ | 0.008 | $H_4^{ERT\text{-}R}$ | -0.006 |
| $H_3ax^{ERT\text{-}C}$ | nd* | $H_4^{ERT\text{-}G}$ | 0.021 | $H_6^{ERT\text{-}R}$ | nd* |
| $H_8^{ERT\text{-}A}$ | 0.051/0.015 | | | | |
| $H_6^{ERT\text{-}A}$ | 0.077/0.057 | | | | |

**Table S3** Complexation shifts ($\Delta\delta$, 600 MHz, $D_2O$, 25 °C) of β-CD protons (1.53 mM) in ERT/β-CD 1:1.

| ERT/β-CD 1:1 | $H_1^{CD}$ | $H_2^{CD}$ | $H_3^{CD}$ | $H_4^{CD}$ | $H_5^{CD}$ | $H_6^{CD}$ | $H_{6'}^{CD}$ |
|---|---|---|---|---|---|---|---|
| $\Delta\delta$ (ppm) | -0.02 | -0.02 | -0.07 | 0.00 | -0.14 | -0.06 | -0.06 |

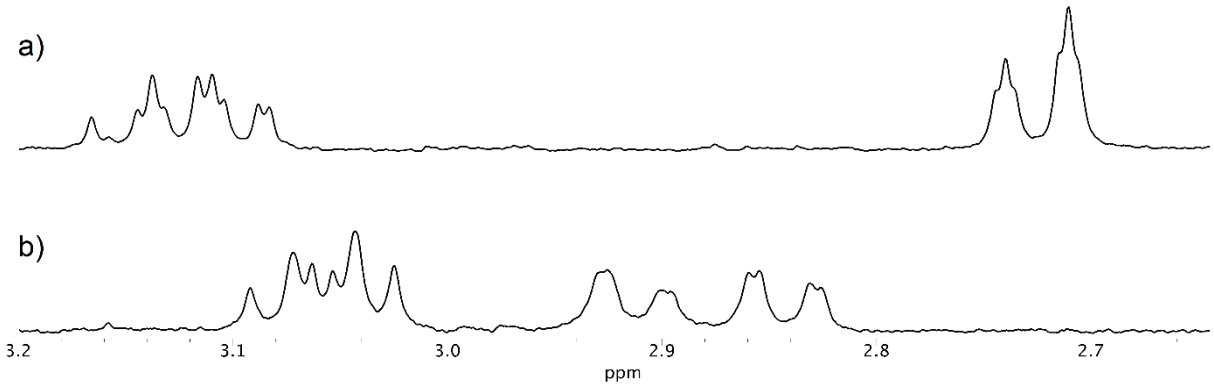


**Figure S7** $^1$H NMR (600 MHz, $D_2O$, 25 °C) spectral region of $H_3^{ERT\text{-}C}$, (a) in absence and (b) in presence of β-CD.

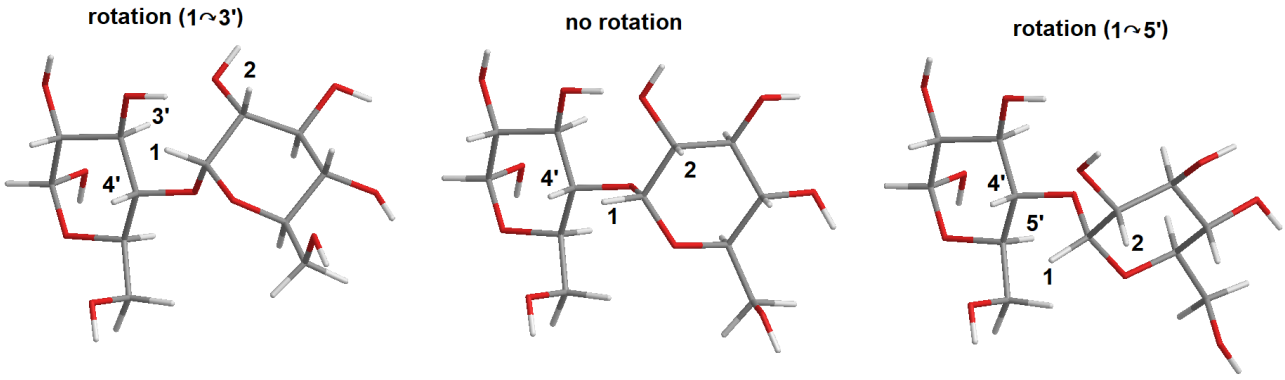


**Figure S8** 3D models of two glucopyranose units describing the possible mutual rotation around glycosidic linkage.

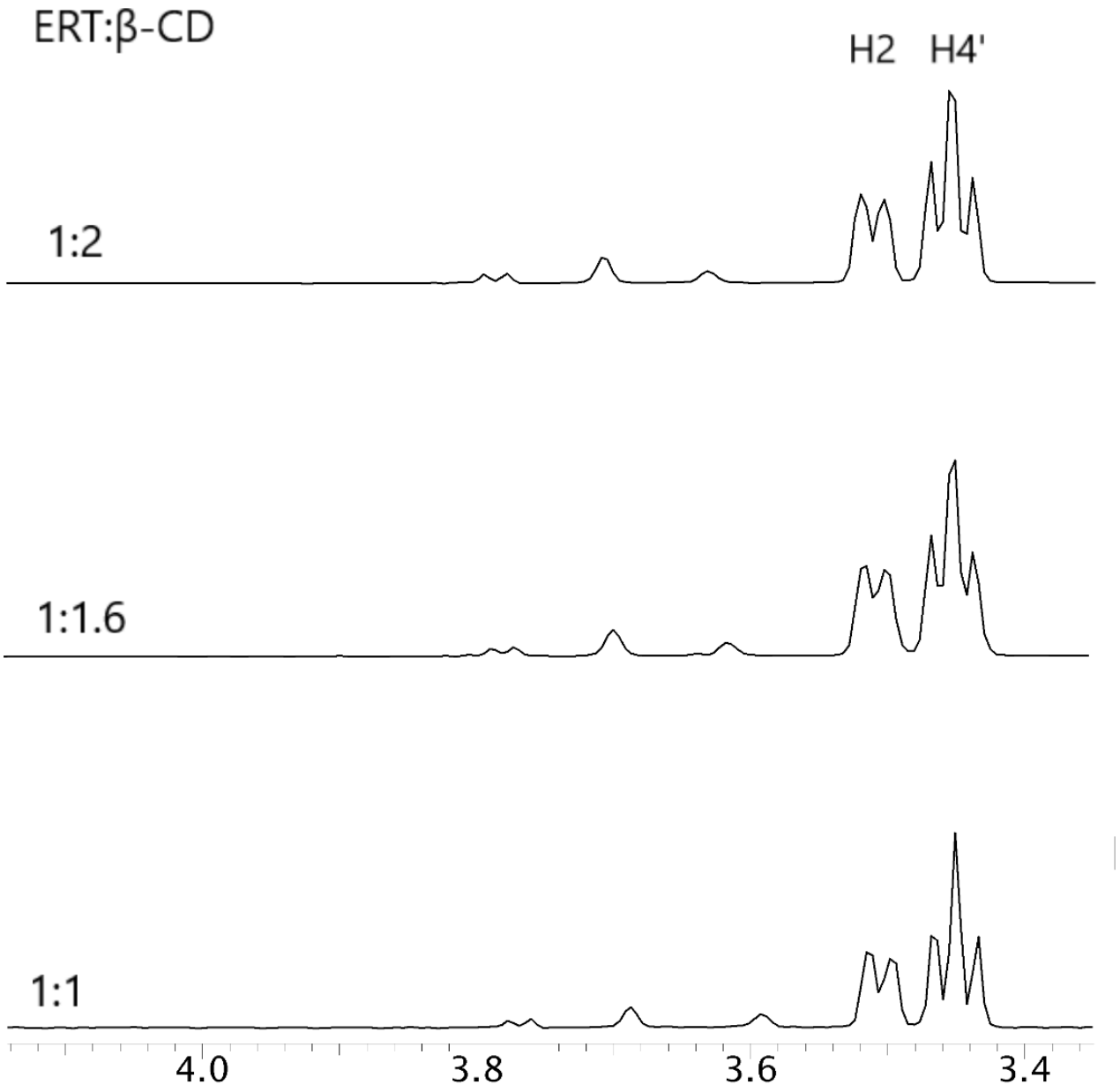


**Figure S9** 2D ROESY traces (600 MHz, $D_2O$, 25 ℃, mix=0.3 s) corresponding to H1 proton of β-CD in ERT/β-CD.

**Table S4** $^1$H NMR (600 MHz, $D_2O$, 25 ℃) chemical shifts ($\delta$, ppm) of free HP-β-CD and its complexation shifts ($\Delta\delta$, ppm) in ERT/HP-β-CD 1:1 mixture.

| Proton | HP-β-CD $\delta$ | ERT/HP-β-CD 1:1 $\Delta\delta$ | Proton | HP-β-CD $\delta$ | ERT/HP-β-CD 1:1 $\Delta\delta$ |
|---|---|---|---|---|---|
| $H^{HP}_{1a}$ | 4.94 | -0.03 | $H^{HP}_{1b}$ | 5.11 | -0.03 |
| $H^{HP}_{2a}$ | 3.51 | -0.02 | $H^{HP}_{2b}$ | 3.36 | 0.03 |
| $H^{HP}_{3a}$ | 3.82 | -0.06 | $H^{HP}_{3b}$ | 3.92 | -0.05 |
| $H^{HP}_{4a}$ | 3.45 | -0.02 | $H^{HP}_{4b}$ | 3.49 | -0.02 |
| $H^{HP}_{5a}$ | 3.72 | -0.14 | $H^{HP}_{5b}$ | 3.71 | -0.08 |
| $H^{HP}_{6a}$ | 3.73 | -0.15 | $H^{HP}_{6b}$ | 3.75 | -0.12 |

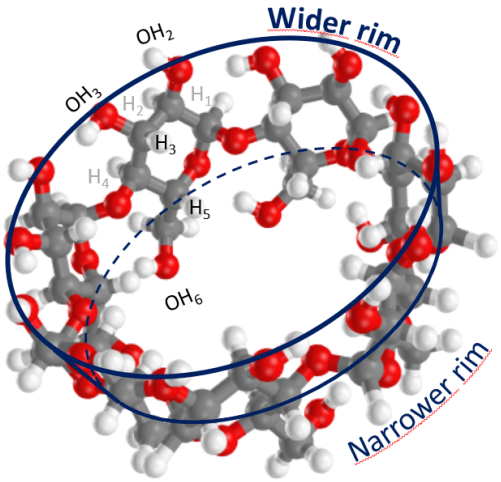


**Figure S10** 3D model of β-cyclodextrin, with protons labeled.

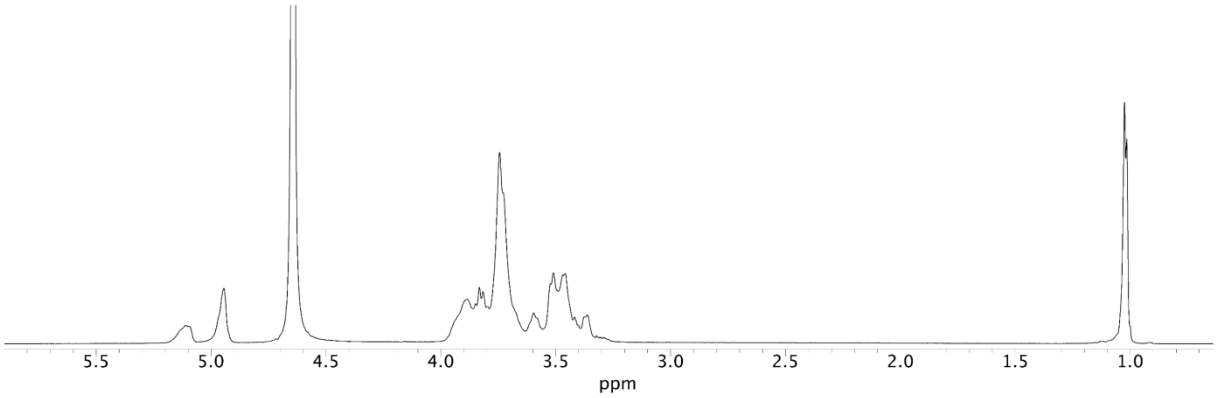


**Figure S11** $^{1}$H NMR (600 MHz, $D_2O$, 25 ℃) of HP-β-CD.

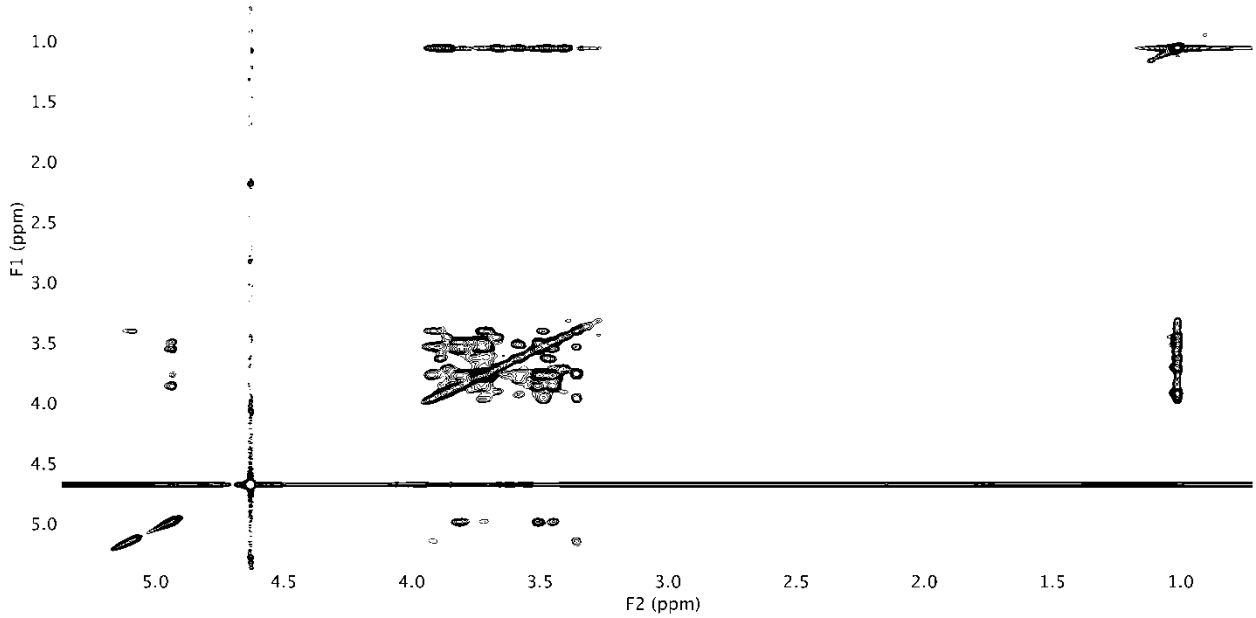


**Figure S12** Portion of 2D TOCSY map (600 MHz, $D_2O$, 25 ℃) of HP-β-CD.

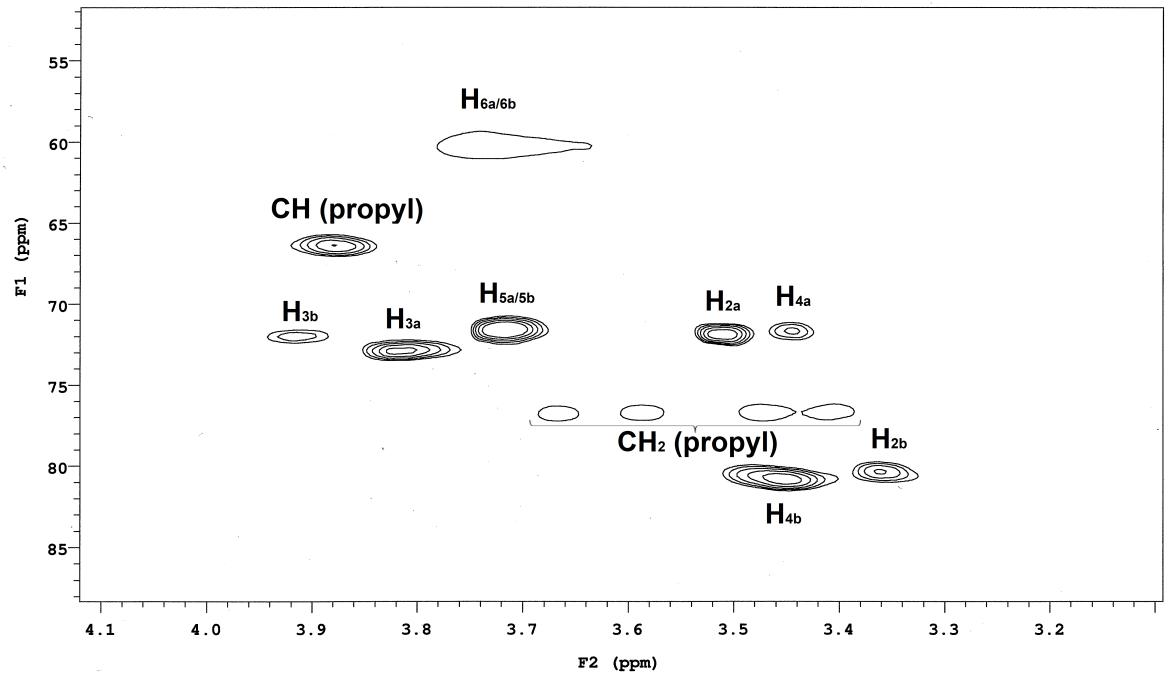


**Figure S13** Portion of 2D gHSQC (600 MHz, $D_2O$, 25 ℃) of HP-β-CD.

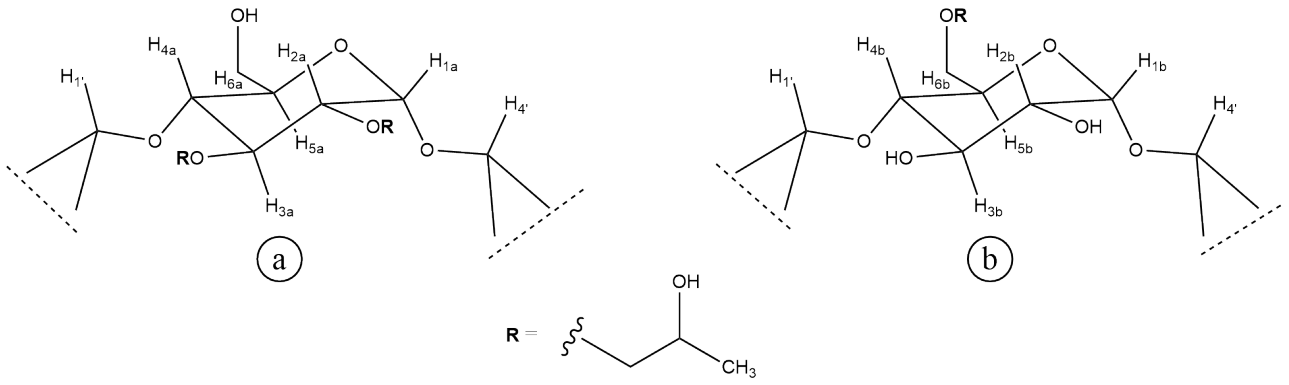


**Figure S14** Chemical structure of two units of HP-β-CD.

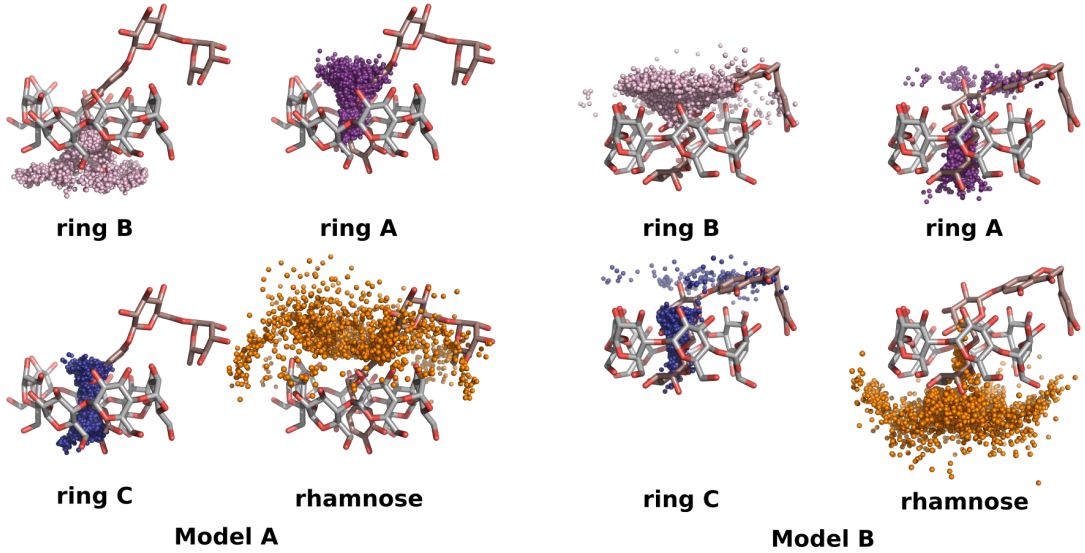


**(a)** β-CD

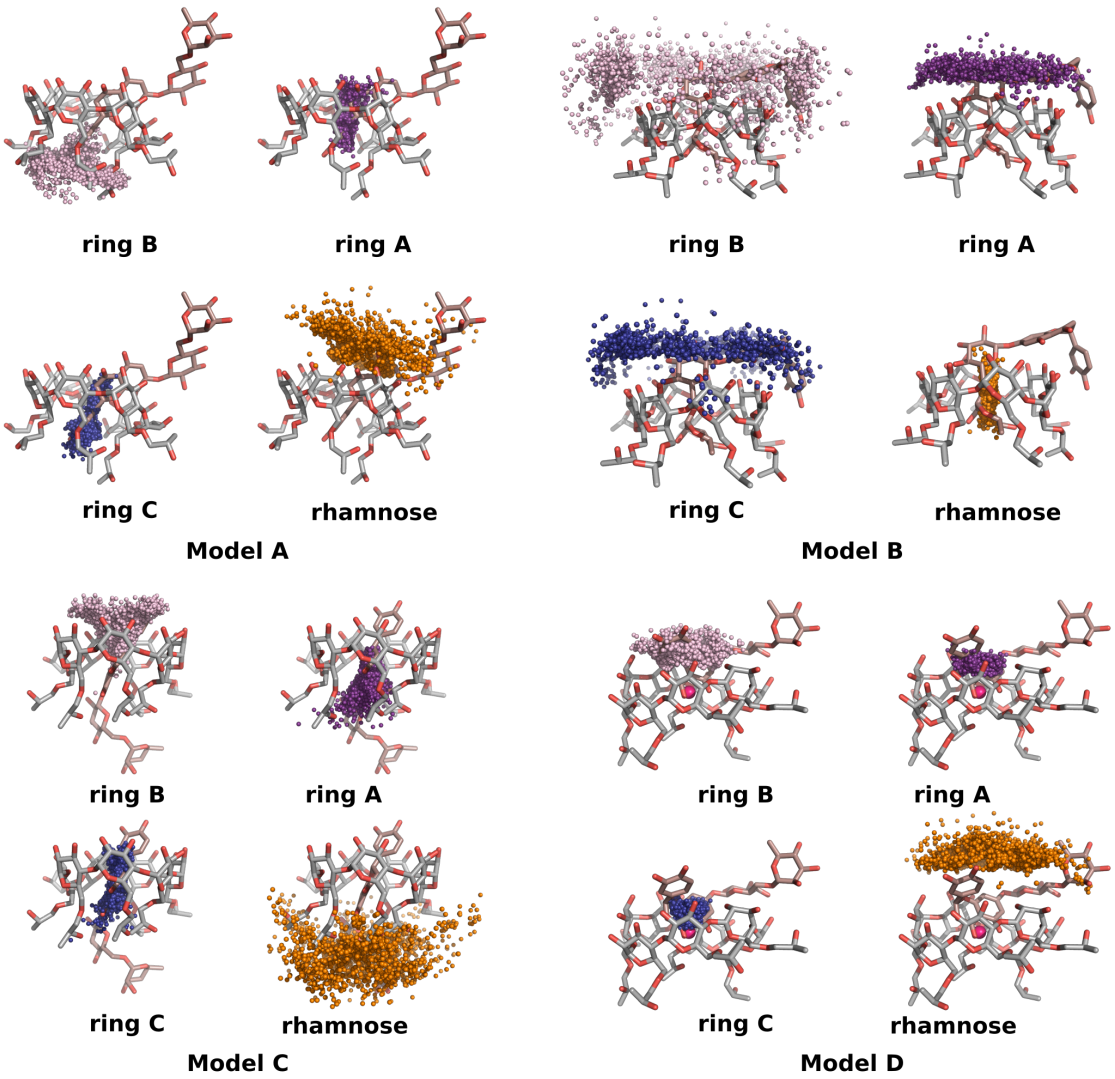


**(b)** HP-β-CD

**Figure S15** The position of ERT's rings A, B and C, plus that for rhamnose's center (defined by its C and O ring atoms) during the (a) β-CD and (b) HP-β-CD 1:1 models' trajectories (with every 100 ps shown), superimposed upon the starting conformations of the production simulations.

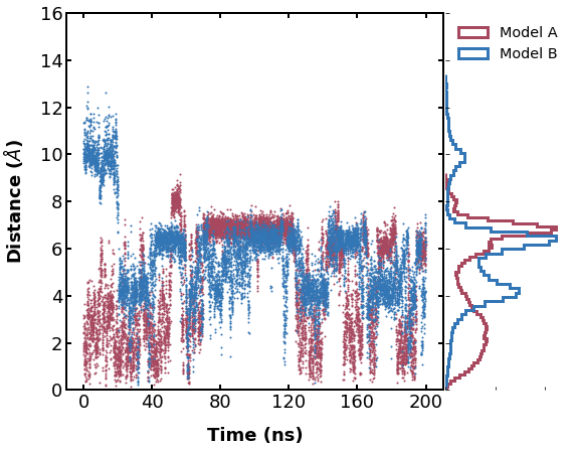


**(a)** ring B

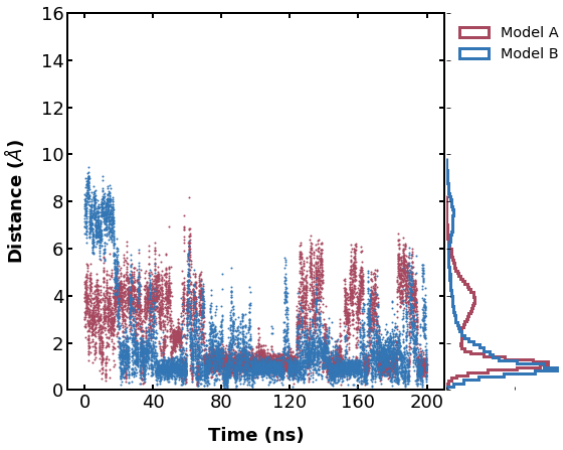


**(b)** ring A

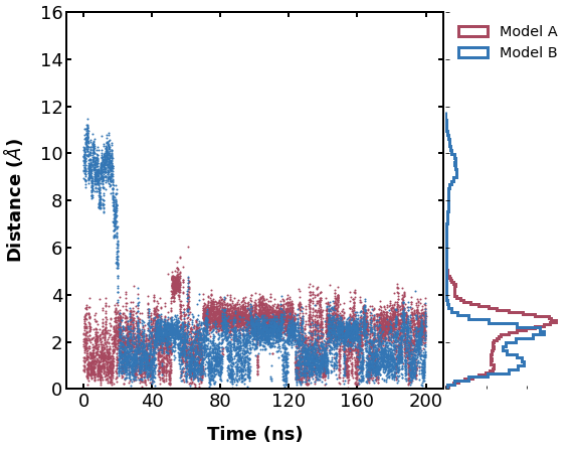


**(c)** ring C

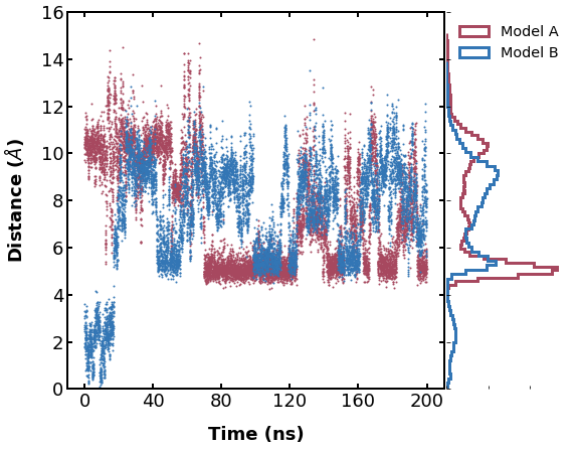


**(d)** rhamanose ring

**Figure S16** The distance between ERT's (a) ring B, (b) ring A, (c) ring C and (d) rhamanose (defined by its C and O ring atoms) to the center of the β-CD of Model A and B. Specifically, the distances between the center of the respective rings and the center of cyclodextrin (defined by the ring atoms of all seven α-D-glucose units) are measured. The scatter plots show every 20$^{th}$ (i.e. every 20 ps) data point, while the histograms represent the full data set.

The change in ring A's distance reflects how deeply ERT is inserted into the β-CD. While ring A and C are connected, ring C is positioned closer to the β-CD's center in Model A (Figures S16b and S16c), and adopts placements both "*above*" and "*below*" β-CD's center (Figure S15a: ring C). Ring A is almost exclusively position towards β-CD's wide rim (i.e. *above* β-CD's center). Consequently, as ring A and C translates up and down within β-CD's cavity, ring C is hindered more than ring A in its side-to-side movement. Our interpretation is that this results in a ring C histogram that is more confined and continuous (Figure S16c) than observed for ring A (Figure S16b). Ring A has more freedom for movement, and adopts diverse placements both near the β-CD's center and near the wide rim – imagine a hallowed, inverted cone shape within β-CD (see Figure S15a: ring A). This leads to the two distinct ring A histogram peaks.

To finish this analysis and as seen in Figure S16a, ring B has an even greater variety of positions that can be adopted due to a) its location that is even further from the β-CD's center (i.e. it is not as confined within β-CD's cavity) and b) the additional puckering flexibility of ring C (i.e. Figure 7: E+ and E-).

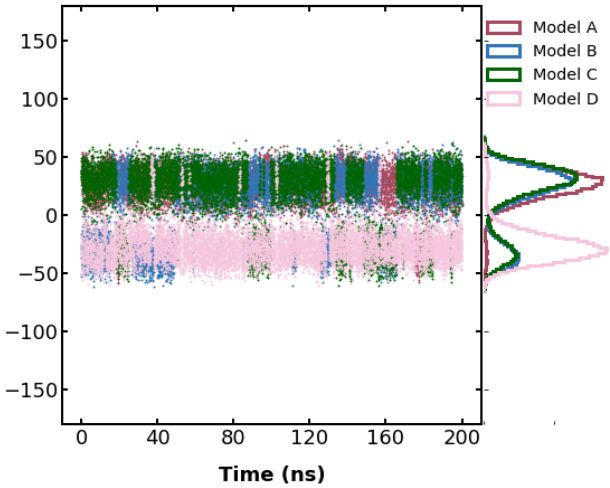


**Figure S17** Distribution of ERT's puckering dihedral angle (i.e. ring C's C-$C_4$-$C_3$-$C_2$) as a function of HP-β-CD's Model A, B, C and D's trajectories. The scatter plot displays every 20$^{th}$ (i.e. every 20 ps) data point, while the histogram represents the full data set.

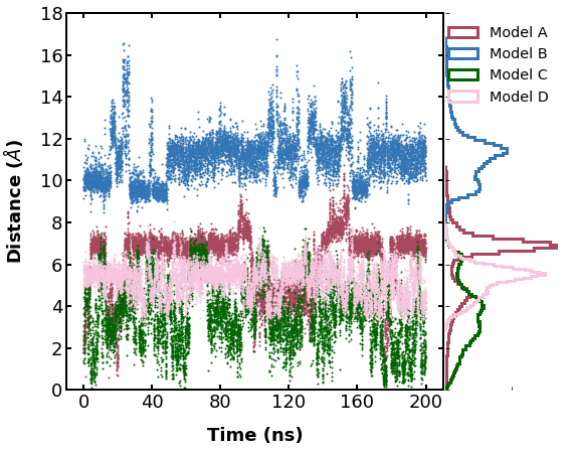


**(a)** ring B

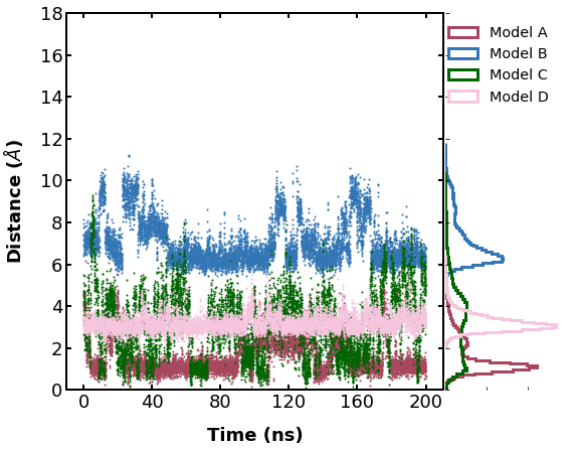


**(b)** ring A

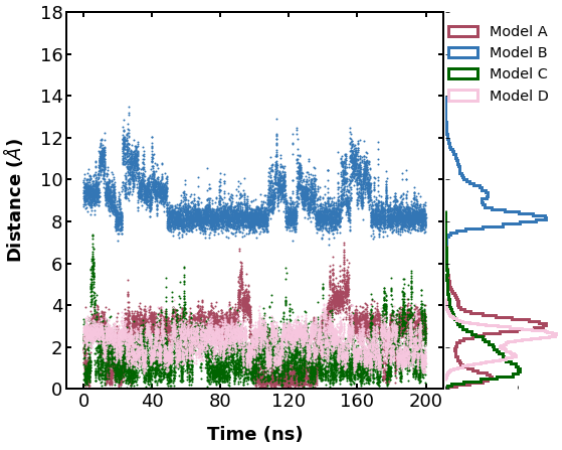


**(c)** ring C

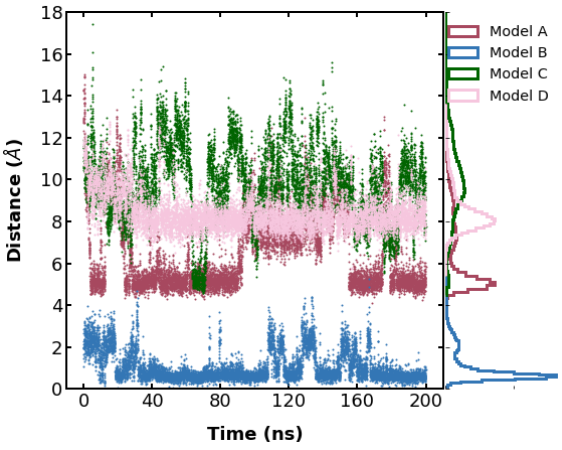


**(d)** rhamanose ring

**Figure S18** The distance between ERT's (a) ring B, (b) ring A, (c) ring C and (d) rhamanose (defined by its C and O ring atoms) to the center of the HP-β-CD of Models A, B, C and D. Specifically, the distances between the center of the respective rings and the center of cyclodextrin (defined by the ring atoms of all seven α-D-glucose units) are measured. The scatter plots show every 20$^{th}$ (i.e. every 20 ps) data point, while the histograms represent the full data set.

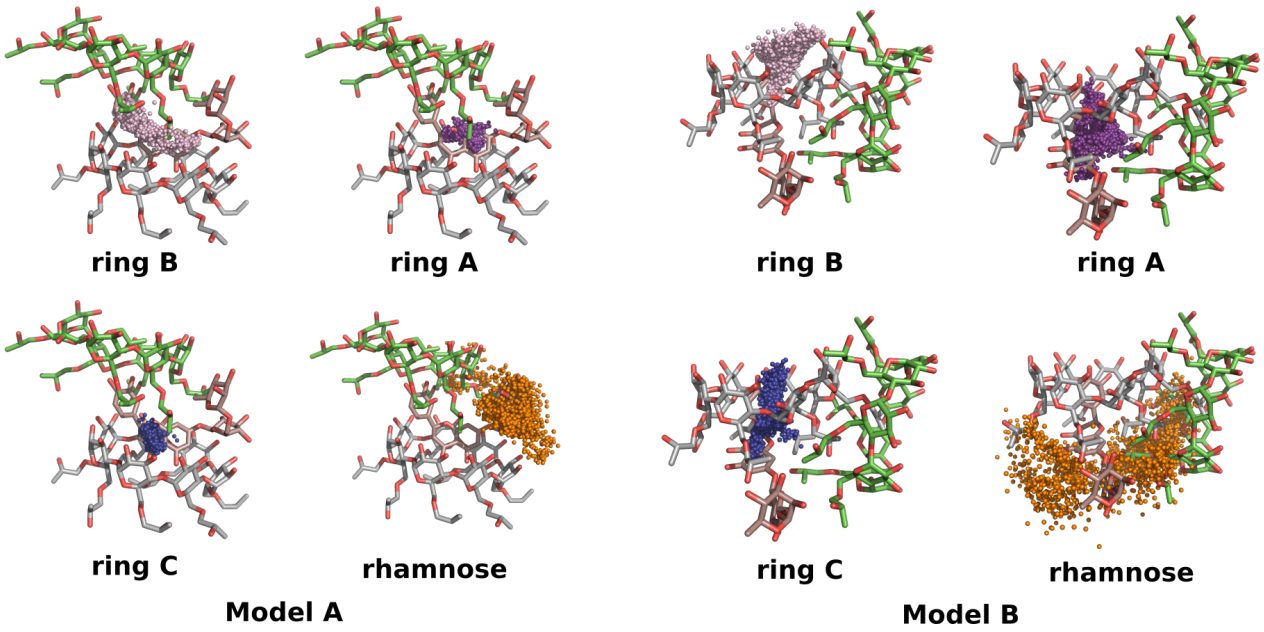


**Figure S19** The position of ERT's rings and rhamnose center during the HP-β-CD 1:2 models' trajectories (with every 100 ps shown), superimposed upon the starting conformations of the production simulations. The primary cyclodextrin is colored grey, while the secondary one is green.

Very early in Model B's simulation (i.e. during the equilibration phase), ERT loses its interaction with the primary HP-β-CD's inner cavity, due to its interactions with the secondary HP-β-CD. Once removed from the cavity, ERT translates along the primary's exterior surface and reinserts itself into the narrow rim (via ring B). Once reinserted, ERT remains within the cavity for the remainder of the simulation (Figure S20). This binding mode is similar to that seen for HP-β-CD 1:1 model C (Figure 11b) - where ring B interacts with the wide rim, and rings A and C position themselves along the central axis formed by the glucose and 2-hydroxylpropyl functional groups (Figure S19).

With this binding mode, two general relative orientations are populated between the two HP-β-CDs. The most frequent interaction is where the narrow rim of the secondary cyclodextrin interacts with the exterior of the primary (Figure S20, clusters 1 and 2). A second orientation is also observed near the end of the simulation, where both cyclodextrins interact through their exterior surfaces (Figure S20, clusters 3). Interestingly, in both Model A and B simulations, a single 2-hydroxylpropyl pendant on the secondary HP-β-CD adopts an orientation that places itself in the center of its cyclodextrin. This does not occur in the primary HP-β-CD (i.e. the cyclodextrin whose cavity binds ERT) due to steric hindrance caused by the ligand. Furthermore, the interior placement of a 2-hydroxylpropyl group appears to facilitates the side–side interaction between the two cyclodextrins since its associated glucose forms the central interface unit.

In summary of these HP-β-CD 1:2 model simulations, the three-body interaction between one ERT and two HP-β-CDs shows complex intermolecular interactions and labile configurations. Out of the six most populated cluster configurations observed from the two ERT/HP-β-CD 1:2 models, cluster 3 of Model A bests represents the NMR data, in addition to ERT/HP-β-CD 1:1's Model D.

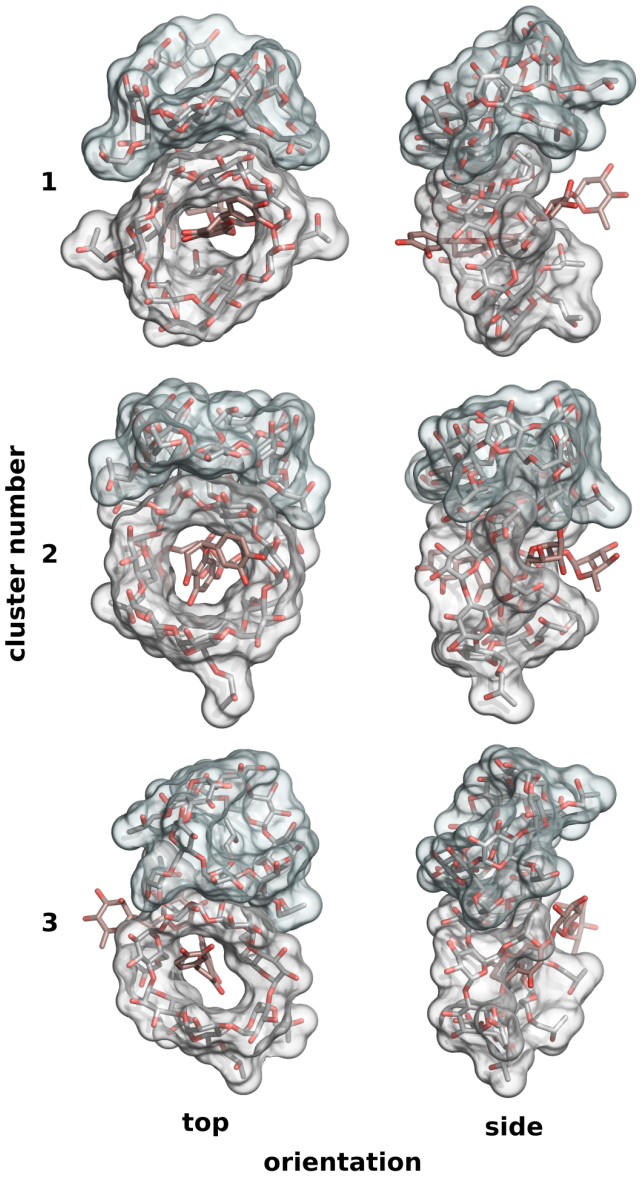


**Figure S20** Mixed rendering of the ERT/HP-β-CD representative structures for the three most populated hierarchical agglomerative clusters of Model B. The bottom cyclodextrin is the primary one.